Fabrication of Silver Vanadium Oxide and V_2O_5 Nanowires for Electrochromics

Chunrong Xiong,[†] Ali E. Aliev,[‡,⊥] Bruce Gnade,[†,§] and Kenneth J. Balkus, Jr.[†,⊥,*]

[†]Department of Chemistry, [‡]Department of Physics, [§]Department of Electrical Engineering, and [⊥]Alan G. MacDiarmid NanoTech Institute, University of Texas at Dallas, Richardson, Texas 75083-0688

ABSTRACT Silver vanadium oxide (SVO) and V_2O_5 nanowires have been hydrothermally synthesized. The as-made nanowires are over 30 μm long and 10–20 nm in diameter. The nanowires have a layered structure with a *d*-spacing of 1.07 nm. The nanowires can be fabricated into free-standing and flexible sheets by suction filtration. The electrical conductivity of the SVO nanowires is 0.5 S/cm, compared to 0.08 S/cm for the V_2O_5 nanowires. The Li ion diffusion coefficient in the SVO nanowires was 7 times higher than that in the V_2O_5 nanowires. An electrochromic device was fabricated from the SVO nanowires that displayed a color-switching time of 0.2 s from the bleached state (green) to the colored state (red-brown) and 60% transmittance contrast.

KEYWORDS: silver vanadium oxide · V_2O_5 · nanowires · electrochromic device

The ease with which V_2O_5 can be reduced and its ions intercalated into layered structures makes it a promising material for applications such as lithium batteries,[1–3] catalysts,[4–6] electrochromic devices (ECDs),[7–9] and supercapacitors.[10–12] Recently, silver-doped V_2O_5 (silver vanadium oxide, SVO) was shown to significantly improve the intercalation rate, specific capacity, and cycling performance in lithium ion batteries.[13] It has also been used in implantable cardioverter defibrillators due to its long-term stability.[14,15] In earlier reports, SVO films were made by pulse laser deposition (PLD),[16–18] sputtering,[19] evaporation, and vapor deposition.[20,21] Bulk SVO was also synthesized by heat, melting a silver salt with vanadium oxide.[22,23] Recently, $Ag_2V_4O_{11}$ nanowires and nanobelts were prepared by a hydrothermal approach.[24,25]

V_2O_5 nanorods and nanowires have attracted attention due to their novel applications as sensors,[26] field-effect transistors,[27–29] electric actuators,[30] and nanolithography templates.[31] V_2O_5 nanowire sheets as actuators display a high Young's modulus, high actuator-generated stress, and high actuator stroke at low applied voltage.[32] Vanadium oxide nanowires have been prepared by several methods. Nesper *et al.*[33] synthesized tubular vanadium oxide by a sol–gel reaction of vanadium alkoxides with a primary amine. Niederberger *et al.*[34] synthesized mixed-valence vanadium oxide nanorods *via* a nonaqueous low-temperature procedure. V_2O_5 nanorods and nanowires have also been synthesized in reverse micelles.[35] Cao *et al.*[36] reported the growth of V_2O_5 nanorod arrays using electrophoretic deposition combined with templating. For these syntheses, the length of the nanowires was usually less than 10 μm. Longer nanowires are expected to facilitate formation of free-standing sheets or films. Hydrated V_2O_5 nanowires, 10 μm long, were synthesized by the polycondensation of vanadic acid in water at room temperature.[32,37] This process requires several weeks due to the slow ion exchange between Na^+ and H^+ ions in a resin from sodium metavanadate solutions at room temperature. In this paper, we introduce a facile method to make high-aspect-ratio SVO and V_2O_5 nanowires with layered structure in one day, where the as-made nanowires are over 30 μm long and ~10−20 nm wide.

V_2O_5 films display a color change when lithium ions are injected into or extracted from the layer spaces by applying a small voltage. V_2O_5 films have been used as a working electrode in ECDs. Traditionally, V_2O_5 films have been made by sputtering,[38] chemical vapor deposition (CVD),[39] vacuum evaporation,[40] and sol–gel processes.[41] To improve the intercalation and extraction kinetics of lithium ions in V_2O_5, a short diffusion distance, bigger interlayer space, and good electrical conductivity are desired.[42] Recently, TiO_2/V_2O_5,[43] Nb_2O_5/V_2O_5,[44] and polyaniline/V_2O_5[45] composite films have been proposed to shorten the

*Address correspondence to balkus@utdallas.edu.

Received for review September 27, 2007 and accepted December 19, 2007.

Published online January 10, 2008.
10.1021/nn700261c CCC: $40.75

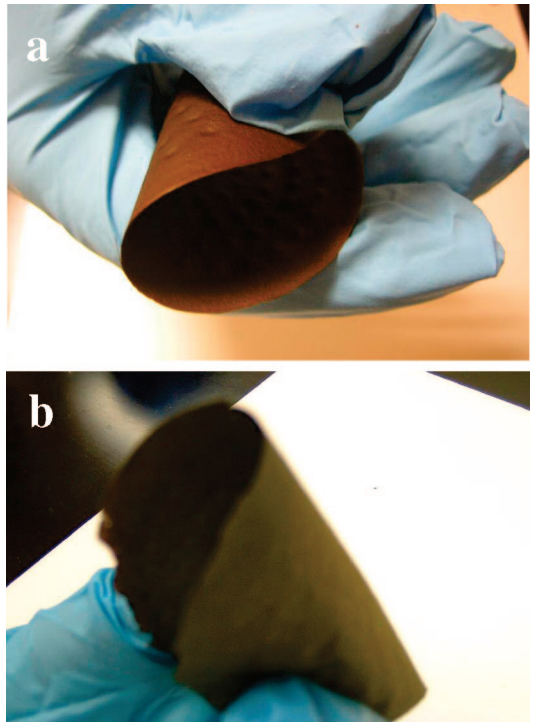

Figure 1. Digital photographs of free-standing sheets fabricated by suction filtration of (a) SVO nanowires and (b) V_2O_5 nanowires.

switching time. Meanwhile, V_2O_5 nanorod and nanowire films have been investigated.[42,46] In this report, an ECD was constructed by dip-coating SVO nanowires onto ITO-coated glass. The resulting device displayed a much shorter color-switching time and a bigger transmittance contrast compared to the V_2O_5 nanowires.

RESULTS AND DISCUSSION

A digital photograph of a free-standing SVO nanowire sheet peeled off a filter paper is shown in Figure 1a. As can be seen in the image, the sheet was brown, and it was flexible and could be folded without breaking. The SVO nanowire paper has potential applications in supercapacitors and actuators. A V_2O_5 nanowire sheet was also fabricated by the same strategy. The free-standing sheet composed of V_2O_5 nanowires was green-brown, as shown in Figure 1b. The green-brown color suggests partial reduction of the V^{5+} in the nanowires. Both sheets were ~50 μm thick. The top-view scanning electron microscopy (SEM) images of the SVO film dip-coated onto ITO glass show that the SVO film comprises entangled nanowires with an aspect ratio of over 1500, 30 μm long and 10–20 nm wide, as can be seen in Figure 2a,b. The SVO film on the ITO glass was ~500 nm thick, as shown in the SEM image of the film cross section in Figure 2c. A V_2O_5 nanowire film with the same thickness was also made by the same method and is shown in Figure 2d. It can be seen from the top-view SEM images in Figure 2e,f that the V_2O_5 nanowires have the same aspect ratio as the SVO nanowires.

The X-ray diffraction (XRD) pattern in Figure 3a reveals that the as-made SVO nanowires matched the $Ag_{0.35}V_2O_5$ phase (PDF No. 00-028-1027) with characteristic peaks at $2\theta = 12.24$, 18.78, 23.25, 25.52, 29.25, 34.48, 46.08, and 50.65°. These peaks can be assigned to (002), (200), (−104), (011), (104), (113), (−504), and (020) lattice planes, respectively. Two weak peaks at $2\theta = 38.1$ and 44.3°, characteristic of Ag metal, can also be found in the XRD pattern of the SVO nanowires. The size of the Ag particles was 3.6 nm, as calculated from the Scherrer equation. The peak at $2\theta = 8.2°$ can be assigned to the (001) reflection, corresponding to a *d*-spacing of 1.07 nm. The XRD pattern of the V_2O_5 nanowires in Figure 2b shows the 00*l* reflections consistent with the layered structure of hydrated V_2O_5.[11,47]

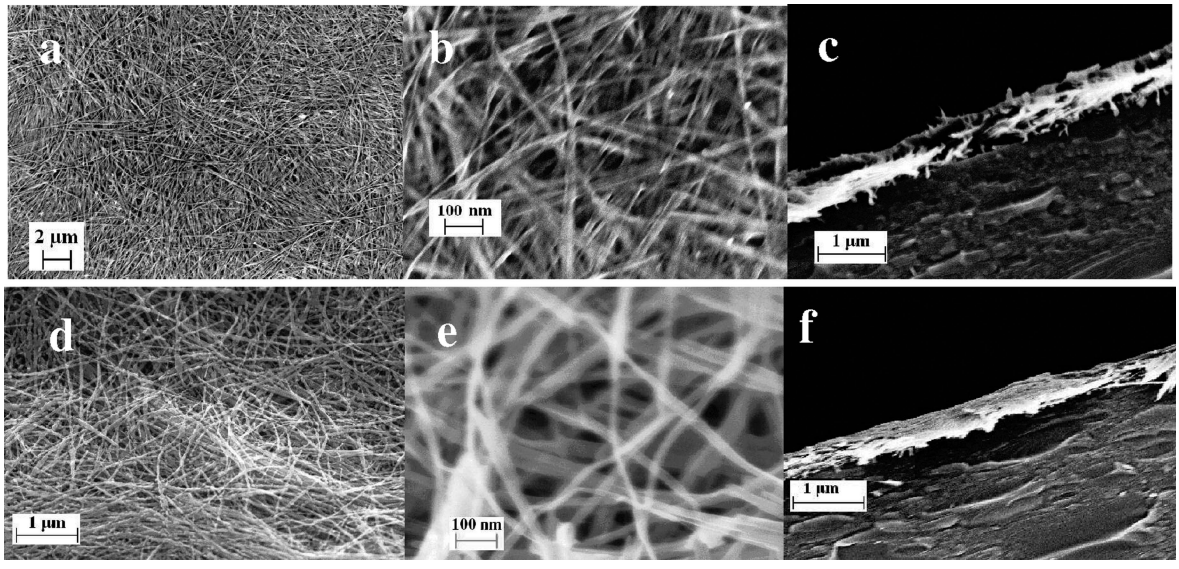

Figure 2. (a,b) Top-view SEM images of a SVO nanowire thin film on ITO glass. (c) SEM image of a cross section of the SVO nanowire thin film on glass. (d,e) Top-view SEM images of a V_2O_5 nanowire thin film on ITO glass. (f) SEM image of a cross section of the V_2O_5 nanowire thin film on glass.

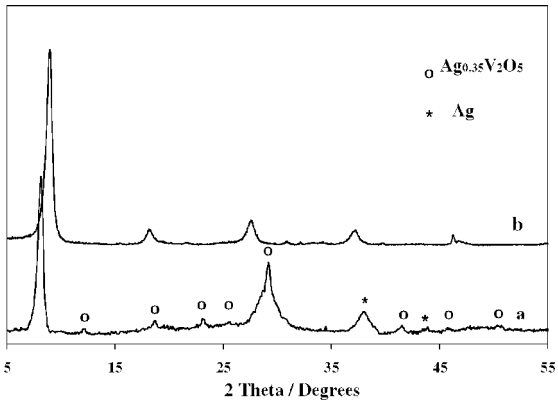

Figure 3. XRD patterns of (a) SVO nanowires and (b) V_2O_5 nanowires.

The peaks at $2\theta = 9.1$, 18.3, 27.7, 37.2, and 46.0° are assigned to (001), (002), (003), (004), and (005) lattice planes, respectively. The *d*-spacing of the V_2O_5 nanowires was 1.01 nm, which is smaller than that for the SVO nanowires in which Ag metal is positioned between or among the V_2O_5 chains spanning the layer space.[37] In the XRD pattern of the V_2O_5 nanowires, four weak peaks at $2\theta = 31.0$, 32.5, 39.8, and 47.2° are also observed. They can be assigned to (200), (131), (022), and (241) lattice planes of NH_4VO_3 (PDF No. 01-076-0191), respectively, which indicates that there were trace amounts of unreacted NH_4VO_3 in the V_2O_5 sample but not in the SVO sample.

To determine the content of coordinated water in the SVO and V_2O_5 nanowires, thermogravimetric analyses (TGA) were carried out. The derivative thermogravimetric curve of SVO nanowires shown in Figure 4a reveals three peaks due to removal of physisorbed and chemisorbed water molecules, as previously reported.[48] The low-temperature weight loss peak at 130 °C may be attributed to the loss of free water. The second weight loss, located at ~235 °C, is due to the loss of physically adsorbed water. For these two low-temperature peaks, the weight losses were 3.8% and 2.7%, respectively, as can be seen in Figure 4b. The maximum peak temperature for weight loss was centered at 350 °C, and the weight loss was 11.2%, which was ascribed to the loss of coordinated water. Thus, the molar ratio of the coordinated water to $Ag_{0.35}V_2O_5$ in the hydrated nanowires may be ~1.14. The derivative thermogravimetric curve shown in Figure 4c also displays three weight loss peaks for the V_2O_5 nanowires at 130, 257, and 400 °C, which correspond to 2.0%, 4.5%, and 12.3% weight loss, respectively. The maximum weight loss peak occurred at 400 °C, 50 degrees higher than that of the SVO nanowires. This is probably because the coordinated water hydrogen-bonds with the oxygens located in the V_2O_5 framework, and embedding of silver in the V_2O_5 framework hinders this interaction. For the V_2O_5 nanowires, the molar ratio of the coordinated water to V_2O_5 was determined to be ~1.25, according to the weight loss curve in Figure 4d.

The transmission electron microscopy (TEM) image of the SVO nanowires displays many silver nanoparticles on the nanowire surface, as can be seen in Figure

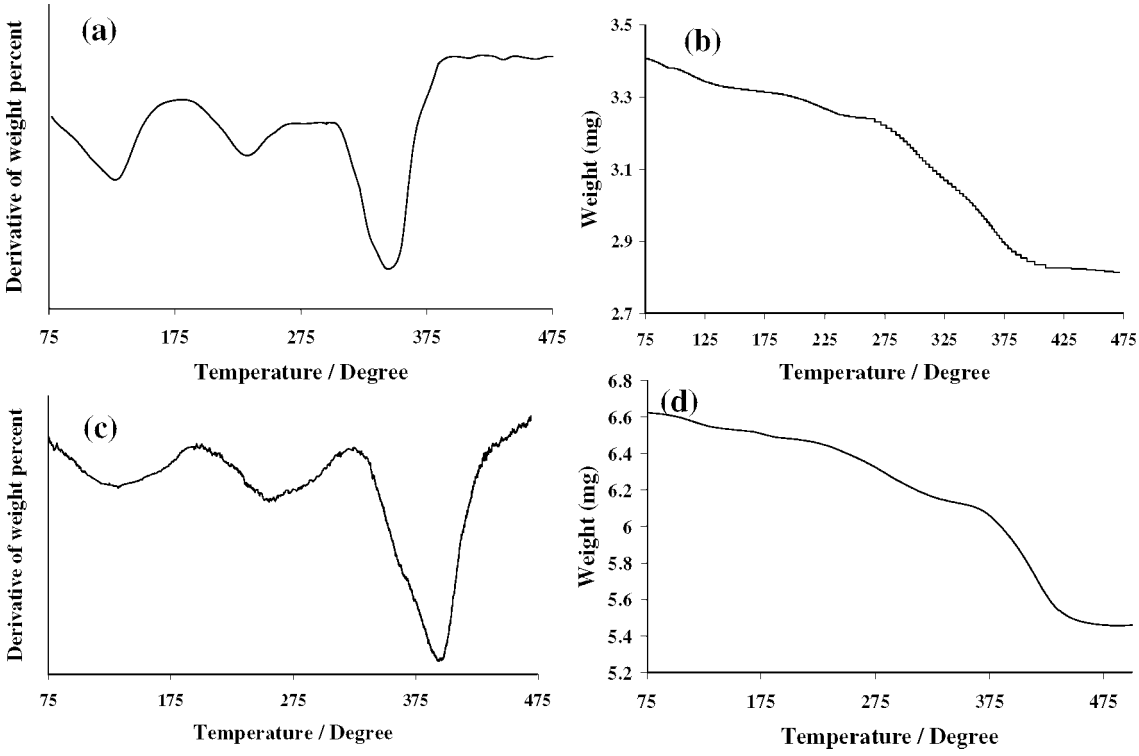

Figure 4. (a) TGA curve and (b) weight loss curve with respect to temperature (°C) for the as-made SVO nanowires. (c) TGA curve and (d) weight loss curve with respect to temperature (°C) for the as-made V_2O_5 nanowires. Test conditions: N_2 flow rate, 20 mL min^{-1}; heating rate, 4 K min^{-1}.

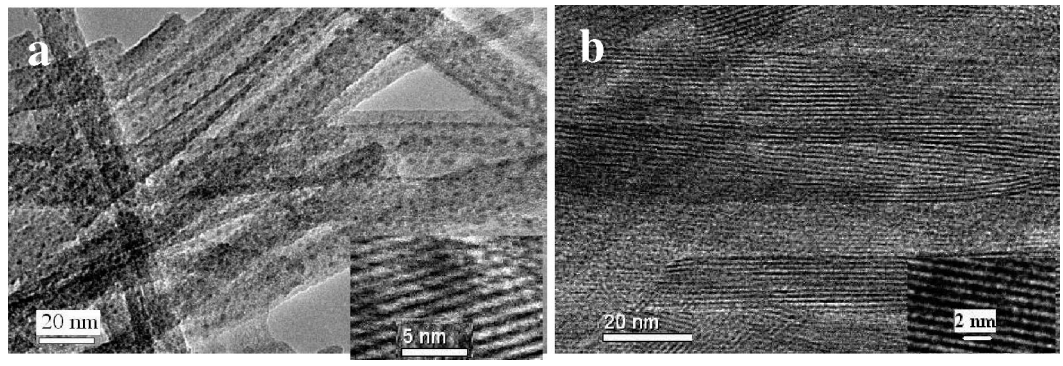

Figure 5. HRTEM images of (a) SVO nanowires and (b) V_2O_5 nanowires. Insets: images with high magnification.

5a. The inset image in Figure 5a shows a layered structure with a lattice spacing of 1.04 nm, a little smaller than that determined from the XRD pattern, probably because of dehydration upon exposure to the high-voltage electron beam under the high-vacuum environment. The nanowires grow along the [010] direction. The crystalline layered structure can also be observed in the V_2O_5 nanowires, as shown in Figure 5b, and the interlayer spacing is 0.97 nm, as determined from the high-resolution (HR) TEM image shown in the inset. The lattice fringes of (001) planes on the nanofibers grow along the fiber growth direction, as previously reported.[9,35]

The FT-IR spectra of the SVO and V_2O_5 nanowires are shown in Figure 6. In both cases, the spectra exhibited characteristic IR bands attributed to V_2O_5. The band centered at 976 cm^{-1} is assigned to the V═O stretching vibration, and the bands at 850 and 542 cm^{-1} correspond to the V—O—V bending vibration and edge-sharing V—O stretching vibration, respectively.[49] In the IR spectrum of the SVO nanowires, the relative intensity of the band at 850 cm^{-1} with respect to the band at 542 cm^{-1} or the band at 976 cm^{-1} decreased compared to that of V_2O_5 nanowires. Such a decrease of the band relative intensity could be due to introduction of Ag^+ into the nanowire framework, which interrupts the V—O—V linkages and produces more

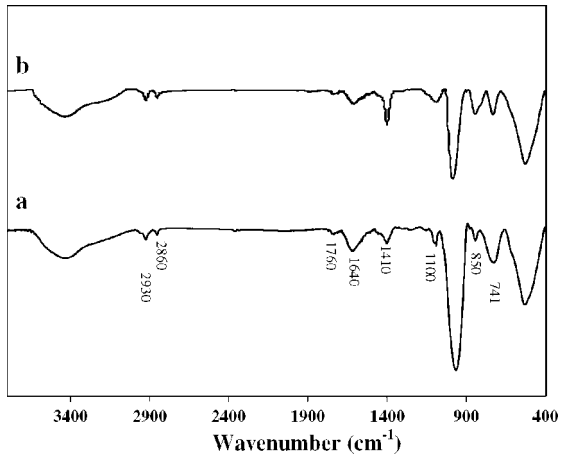

Figure 6. FT-IR spectra of (a) SVO nanowires and (b) V_2O_5 nanowires.

edge-sharing V—O bonds and terminal V═O bonds.[50] The band at 741 cm^{-1} could be assigned to a V—OH_2 stretching mode due to coordinated water.[51] Two IR bands at 3470 and 1640 cm^{-1} are attributed to stretching and bending vibrations of water molecules.[52] The bands at 1100 cm^{-1} in the spectra are related to —OR groups of the organic P123, which indicated that trace organics could be present inside the interlayer space of the nanowires, although the nanowires were sufficiently washed with water and acetone. Additionally, the bending vibration of —CH_2 is also observed at 1410 cm^{-1}, and the bands at 2930 and 2860 cm^{-1} correspond to the asymmetrical and symmetrical stretching bands of —CH_2, respectively. Although there was trace organic existing in the nanowires, it was not observed as an obvious weight loss peak in thermogravimetric analyses, because most weight loss was caused by complexed water, which could hide the contribution of organics. Intercalation of P123 could play a structure-directing role in the preparation of high-aspect-ratio nanowires, as reported by others.[53,54] Moreover, P123 also may act as a reductant to reduce Ag^+ to Ag, along with partial reduction of V^{5+} to V^{4+} during the hydrothermal condensation. X-ray photoelectron spectroscopy (XPS) showed the main binding energy of the V2p3/2 electrons located at 517.5 eV, as can be seen in Figure 7a, suggesting a 5+ oxidation state for most of the vanadium ions. In addition, a small peak at 516.2 eV indicates partial reduction of the V^{5+} ions to V^{4+} during the hydrothermal condensation. The molar ratio of V^{4+} to V^{5+} was 0.11 for the SVO nanowires and 0.14 for the V_2O_5 nanowires. In the XPS spectra of both SVO and V_2O_5 nanowires (as shown in the Supporting Information), the peak at 289 eV suggests formation of some carbonate groups due to oxidation, which is further supported by the band at 1760 cm^{-1}, assigned to C═O groups, shown in Figure 6. The XPS spectrum in Figure 7b shows that the silver species in the SVO sample include Ag^+ and metallic Ag, and the atomic ratio of Ag^+ to Ag is 0.13. It was reported that the Ag-doped $Ag_{0.35}V_2O_5$ phase contains both Ag^0 and Ag^+,[16,18,50] but the atomic ratio of Ag^+ to Ag^0 in the SVO was not reported. The XRD pattern reveals that metallic Ag nanoparticles and $Ag_{0.35}V_2O_5$ coexist in the

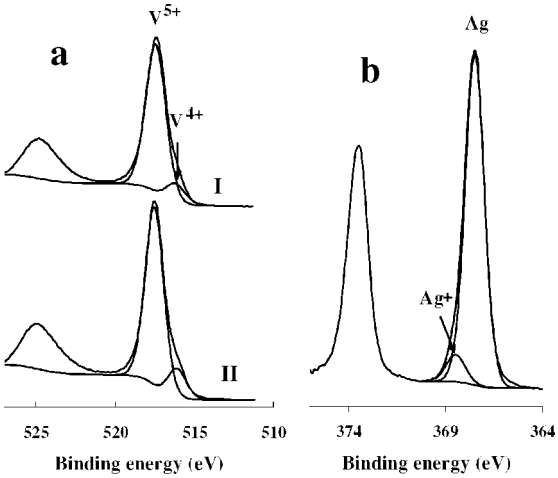

Figure 7. XPS spectra of (a) V2p for (I) the SVO and (II) V_2O_5 nanowires and (b) Ag3d for the SVO nanowires.

sample. To evaluate the atomic ratio of Ag^+ to metallic Ag in the $Ag_{0.35}V_2O_5$ phase, it is necessary to determine the molar ratio of Ag in the metallic Ag nanoparticles covering the SVO nanowires *versus* intercalated or framework Ag in the SVO ($Ag_{0.35}V_2O_5$) nanowires. The atomic ratio of total silver to vanadium in the sample was determined by energy-dispersive spectrometry (EDS) to be 0.244, so the molar ratio of Ag in the metallic Ag nanoparticle phase to that in the SVO ($Ag_{0.35}V_2O_5$) nanowires was 0.39 by calculation. This assumes the SVO phase has a ratio of $Ag_{0.35}V_2O_5$, which is reasonable because if the Ag ratio changes by a small amount, such as $Ag_{0.33}V_2O_5$, then the XRD pattern changes.[19] The atomic ratio of Ag^+ to metallic Ag in the SVO nanowires can be calculated to be 0.23, and the chemical composition of SVO ($Ag_{0.35}V_2O_5$) could be $Ag^+_{0.08}Ag^0_{0.27}V^{5+}_{1.78}V^{4+}_{0.22}O_x$.

Nanowires having a layered structure are very interesting due to their short diffusion distance, which allows reversible intercalation of a variety of ions. Electrochromic devices were made from the as-made nanowires. The bleaching (oxidized) and coloration (reduced) states of the SVO-based ECD are red-brown and green, respectively, as shown in Figure 8a,b. Although the V_2O_5 nanowire sheet looks green-brown in Figure 1b, the nanowire-based ECD also displayed a red-brown color after one cycle of color-switching, because the vanadium was completely oxided to V^{5+} under the applied voltage. The "SVO" and "V_2O_5" labels behind the ECDs can be clearly seen through the nanowire films. Figure 9 shows the optical transmittance spectra of both states for SVO and V_2O_5 nanowire-based ECDs. Each state was scanned five times with an interval of 25 min. For the SVO nanowire-based ECD, the bleached state is very stable, and all spectra almost overlap, as can be seen in Figure 9a. However, in the colored state, the transmittance of the ECD increased with time, indicating that the reduced state was not very stable because Ag nanoparticles could promote catalytic

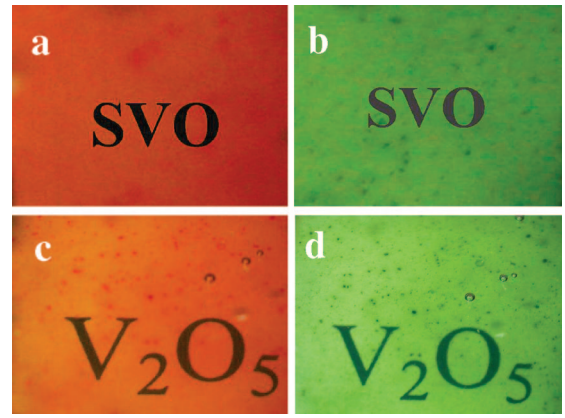

Figure 8. Digital photographs of (a) bleached and (b) colored states for a SVO nanowire-based ECD and (c) bleached and (d) colored states for a V_2O_5 nanowire-based ECD.

oxidation.[55,56] The maximum transmittance change, ΔT, was 60% at 1020 nm. The UV–vis transmittance spectra of the V_2O_5 nanowire-based ECD displayed good stability in both states, as can be seen in Figure 9b. The maximum ΔT was 33.7% at 1005 nm.

The color-switching time of the ECD was measured by a Si photosensor. The EDC with SVO nanowires deposited on ITO glass as an anode and ITO glass as counter electrode was very stable in the applied voltage window from -2.5 to $+3.8$ V. The applied voltage *vs* time plot shown in Figure 10 displays the coloration-bleaching processes: $U = -1.5$ V for bleaching (green color) and $U = 2.5$ V for coloration (red-brown color). The color-switching time, defined as half the total transmittance change, was about 0.2 s from green to red-

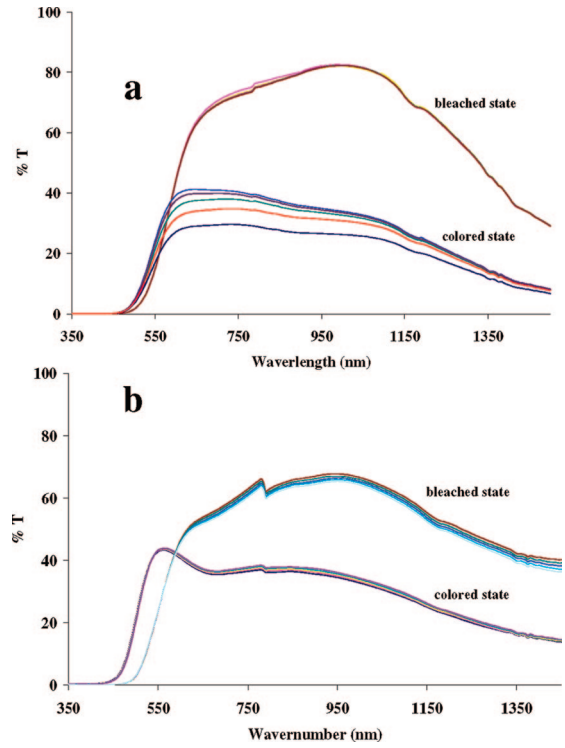

Figure 9. Optical transmittance spectra of (a) a SVO nanowire ECD and (b) a V_2O_5 nanowire ECD.

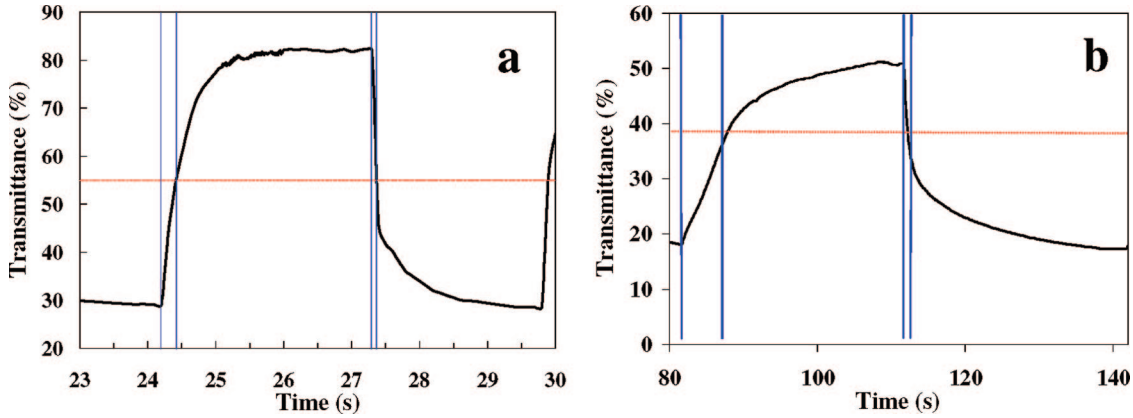

Figure 10. Transmittance *vs* time during coloration and bleaching cycles of (a) a SVO nanowire-based ECD and (b) a V_2O_5 nanowire-based ECD.

brown and 0.1 s for the reverse process at 633 nm, as shown in Figure 10a. For V_2O_5 nanowires, the color-switching time was 6 s from green to brown and 1 s for the reverse process, as shown in Figure 10b, apparently much slower than that for SVO nanowires. Cheng *et al.*[46] reported the color-switching time of a V_2O_5 nanowire ECD to be 6 s from the colored state to the bleached state and 5 s from the bleached state to the colored state. Takahashi *et al.*[9] reported that a 30% transmittance change at 700 nm took 50 s for a V_2O_5 nanorod ECD when 3.0 V was applied, and 300 s was required for a sol–gel V_2O_5 ECD. For electrochromic applications, immediate color-switching is important. The rates of coloring and bleaching depend on the lithium ion diffusion rate and the diffusion distance in the interlayer space of the nanowires. In our case, both the SVO and V_2O_5 nanowires are 10–20 nm wide, which provides a short diffusion distance. In the reported V_2O_5 nanowire or nanorod ECDs, the diameter sizes were ~100 nm.[9,46] Moreover, the SVO nanowire sheets are more electroconductive (0.5 S/cm) than the V_2O_5 nanowire sheets (0.08 S/cm), and the SVO nanowires have a bigger interlayer spacing (1.04 nm) than the V_2O_5 nanowires (0.97 nm), which may contribute to a higher Li diffusion coefficient in the SVO nanowires than in the V_2O_5 nanowires.

To evaluate the Li ion diffusion coefficient in the SVO and V_2O_5 nanowires, cyclic voltammetry (CV) was

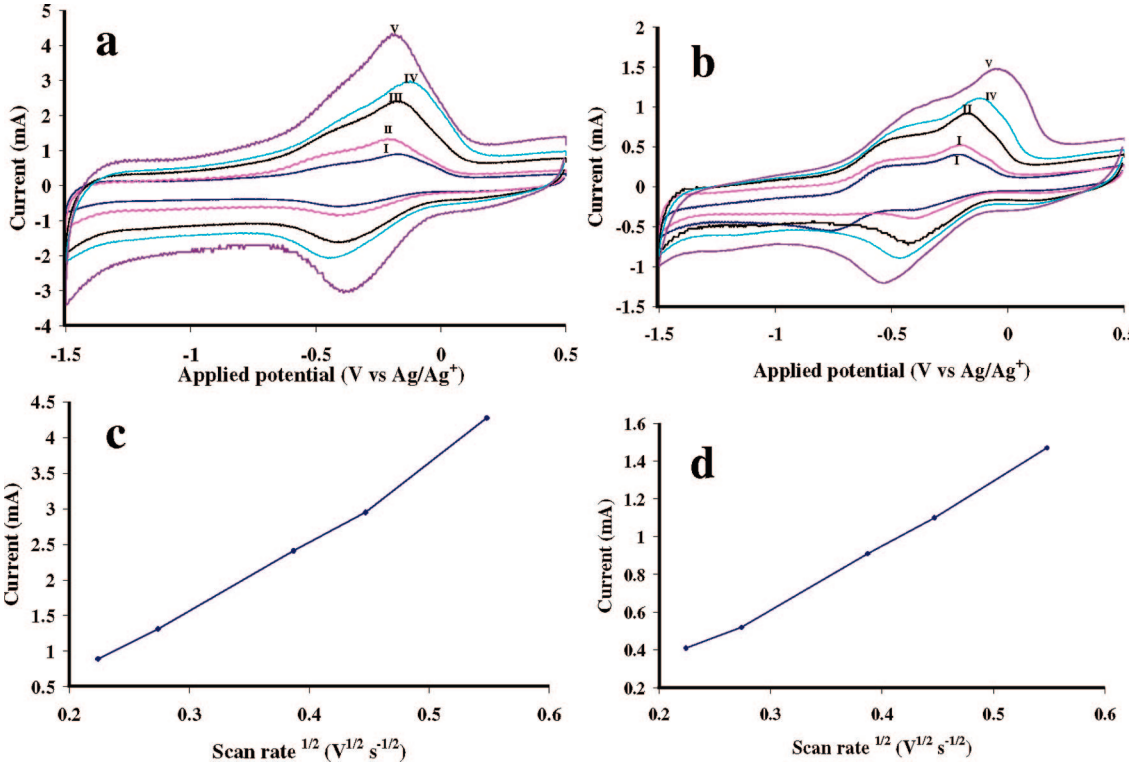

Figure 11. Cyclic voltammograms of (a) SVO nanowires and (b) V_2O_5 nanowires. The scan rates of traces I, II, III, IV, and V are 50, 75, 150, 200, and 300 mV s^{-1}, respectively. Plots of peak current (i_p) as a function of the square root of the scan rates ($v^{1/2}$) for (c) the SVO nanowires and (d) the V_2O_5 nanowires.

carried out with different potential scanning rates on the ~500 nm thick SVO and V_2O_5 nanowire thin films coated on ITO glass. Two oxidation peaks can be seen at −0.15 and −0.45 V in Figure 8a. As reported in the literature,[57,58] V^{4+} ions were partially oxidized first, leaving a mixture of V^{4+} and V^{5+}. The remaining V^{4+} ions were further oxidized to V^{5+} at −0.15 V. This was associated with a different crystalline phase of $Li_xV_2O_5$.[57] The reverse reactions take place, as indicated by the two corresponding reduction peaks at −0.2 and −0.45 V. The Li ion diffusion coefficient can be calculated from a linear relationship between i_p and $v^{1/2}$ according to the following equation,[59]

$$i_p = (2.69\times10^5)\, n^{3/2} a D_{Li}^{1/2} C_{Li}^{*} v^{1/2}$$

where i_p is the peak current (A), a is the electrode area (cm^2), D_{Li} is the apparent diffusion coefficient of the Li^+ ion in the electrode ($cm^2\ s^{-1}$), C_{Li} is the bulk concentration of the Li^+ ion in the electrode (mol cm^{-3}), and v is the potential scan rate (V s^{-1}).

By using CV, the kinetic response was examined to determine the dependence of peak currents on scan rates. Cyclic voltammograms of the SVO nanowire film were obtained at various sweep rates, as shown in Figure 11a. Figure 11c shows a good linear relationship between i_p and $v^{1/2}$ at scan rates lower than 300 mV s^{-1}. The diffusion coefficient of the Li^+ ion in the SVO thin film was estimated to be 5.3×10^{-10} $cm^2\ s^{-1}$. For the V_2O_5 nanowire thin film, the diffusion coefficient of the Li ions was 7.5×10^{-11} $cm^2\ s^{-1}$ according to the linear relationship shown in Figure 11d. The SVO nanowires have a Li diffusion coefficient 7 times higher than that of the V_2O_5 nanowires. Lantelme *et al.*[60] reported that the lithium diffusion coefficient was 10^{-12}–10^{-13} $cm^2\ s^{-1}$ in a V_2O_5 thin film deposited by atomic layer CVD. McGraw *et al.*[61] reported that the maximum diffusion coefficient was 1.7×10^{-12} $cm^2\ s^{-1}$ in an amorphous V_2O_5 film prepared by PLD. Julien *et al.*[62] gave a value of $\sim10^{-12}$ $cm^2\ s^{-1}$ for flash-evaporated V_2O_5 films. Seman *et al.*[63] reported a diffusion coefficient of $\sim1 \times 10^{-11}$–2×10^{-12} $cm^2\ s^{-1}$ for a V_2O_5 thin film deposited by plasma-enhanced CVD. Therefore, the Li ion diffusion coefficient for the SVO nanowires may be the fastest reported for a V_2O_5 system.

CONCLUSIONS

Layered silver vanadium oxide nanowires with a high aspect ratio have been hydrothermally synthesized. The 10–20 nm wide nanowires have a short Li ion diffusion distance. The SVO nanowires have a better electrical conductivity (0.5 S/cm) than V_2O_5 nanowires (0.08 S/cm) prepared using the same method. Introduction of Ag atoms in the V_2O_5 framework further enlarged the interlayer spacing as well as coordinated water. These contributed to a Li ion diffusion coefficient for SVO nanowires that was 7 times higher than that of V_2O_5 nanowires. A faster Li ion diffusion coefficient could make the SVO nanowires a promising material in applications that include Li ion batteries, supercapacitors, and electrochromic devices. The SVO nanowire-based ECD displayed color-switching over 20 times faster than that of the V_2O_5 nanowire-based ECD in our experiments and the literature reports.

METHODS

Preparation of SVO and V_2O_5 Nanowires. SVO nanowires were prepared by the hydrothermal polycondensation of ammonium metavanadate (Aldrich) and reduction of $AgNO_3$ in an autoclave. In a typical synthesis, 0.3 g of ammonium metavanadate and 0.50 g of P123 ($EO_{20}PO_{70}EO_{20}$) were dissolved in 30 mL of deionized (DI) water containing 2 mL of 1 M HNO_3. This mixture was stirred at room temperature for 7 h, and then 1.1 g of $AgNO_3$ was added. After stirring for 1 h, the mixture was transferred to a 50 mL Teflon-lined autoclave and heated to 120 °C for 24 h. The resulting precipitate was dispersed in 50 mL of DI water with vigorous stirring. The product was suction-filtered and rinsed with DI water and acetone. The nanowires were dried at 80 °C for 12 h. The SVO can be peeled off the filter paper as a sheet. For comparison purposes, V_2O_5 nanowires were prepared with the same procedure: 0.3 g of ammonium metavanadate and 0.50 g of P123 were dissolved in 30 mL of DI water containing 1.5 mL of 2 M HCl instead of HNO_3. This mixture was stirred at room temperature for 7 h and then transferred to an autoclave and heated to 120 °C for 24 h. The resulting precipitate was treated by the same process as that used to make the SVO nanowire sheet.

Electrochromic Device. First, 0.25 g of nanowires was dispersed into 20 mL of DI water with vigorous stirring at room temperature, and the solution was concentrated to 5 mL by solvent evaporation at room temperature. The suspension was dip-coated onto ITO glass and dried at 80 °C for 10 min. The ECDs were fabricated by mounting a 1 mm thick adhesive tape on the four sides of the nanowire thin film on ITO glass, and then another ITO glass was placed on top of the tape, leaving a 1 mm thick space, as shown in Figure 12. Finally, 1 M lithium perchlorate in propylene carbonate (PC) electrolyte was injected into the mounted cell until all air was replaced.

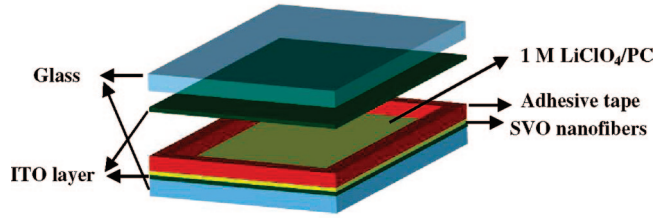

Figure 12. Setup of the electrochromic device (ECD).

Characterization. XRD patterns were collected using a Scintag XDS 2000 X-ray diffractometer with Cu Kα radiation. FT-IR spectra were recorded from KBr pellets between 400 and 4000 cm^{-1} using an Nicolet Avatar 360 FT-IR spectrometer. Scanning electron micrographs were recorded using a LEO 1530 VP field emission scanning electron microscope. The atomic ratio of Ag to V was determined using EDS analysis with Genesis microanalysis software combining energy-dispersive analysis of X-rays (EDAX) algorithms for standardless quantification. The microstructure of the nanowires was observed by TEM using an FEI CM200 FEG transmission electron microscope at 200 kV. XPS analyses were conducted on a PHI5701 LSci instrument with monochromated Al Kα 1486.6 eV as the X-ray source. The takeoff angle was 65°,

and the analysis area was 2.0 × 0.8 mm. The calculation of the atomic ratio of Ag^+ to Ag was based on the area ratio of the binding energy peaks. Cyclic voltammograms were measured using an EG&G Princeton Applied Research potentiostat/galvanostat (model 273A). The nanowire-coated ITO glass served as working electrode, Pt was used as the counter electrode, and Ag/AgCl was used as the reference electrode. The electrolyte was 1 M $LiClO_4$/PC. The optical transmittance spectra of nanowire ECDs were recorded from 350 to 1500 nm using a Perkin-Elmer Lambda 900 UV–vis−NIR spectrophotometer with the ITO-coated glass/electrolyte/ITO-coated glass as a reference. The color-switching of the ECDs as a function of time was measured by using a Si photosensor with a sun imitator lamp as a light source. The EDC with SVO nanowire deposited on ITO-coated glass was used as an anode, and ITO-coated glass was the counter electrode. The electrical conductivity of the nanofiber sheets was measured using a four-point technique, in which four equally spaced probes were placed in contact with the sheet, and then a known current was passed through the outside probes and the voltage was sensed at the two inside probes using a Keithly 2000 multimeter.

Acknowledgment. We gratefully acknowledge financial support from the Robert A. Welch Foundation and SPRING.

Supporting Information Available: XPS spectra of C1s for the SVO and V_2O_5 nanowires. This information is available free of charge *via* the Internet at http://pubs.acs.org.

REFERENCES AND NOTES

1. Poizot, P.; Grugeon, S.; Dupont, L.; Tarascon, J. M. Nano-Sized Transition-Metal Oxides as Negative-Electrode Materials for Lithium-Ion Batteries. *Nature* **2000**, *407*, 496–499.
2. Julien, C.; Haro-Poniatowski, E.; Camacho-López, M. A.; Escobar-Alarcón, L.; Jiménez-Jarquín, J. Growth of V_2O_5 Thin Films by Pulsed Laser Deposition and Their Applications in Lithium Microbatteries. *Mater. Sci. Eng., B* **1999**, *65*, 170–176.
3. Takahashi, K.; Limmer, S. J.; Wang, Y.; Cao, G. Synthesis and Electrochemical Properties of Single-Crystal V_2O_5 Nanorod Arrays by Template-Based Electrodeposition. *J. Phys. Chem. B* **2004**, *108*, 9795–9800.
4. Ponzi, M.; Duschatzky, C.; Carrascull, A.; Ponzi, E. Obtaining Benzaldehyde via Promoted V_2O_5 Catalysts. *Appl. Catal., A* **1998**, *169*, 373–379.
5. Sun, Q.; Jehng, J. M.; Hu, H.; Herman, R. G.; Wachs, I. E.; Klier, K. In Situ Raman Spectroscopy During the Partial Oxidation of Methane to Formaldehyde over Supported Vanadium Oxide Catalysts. *J. Catal.* **1997**, *165*, 91–101.
6. Banares, M. A. Supported Metal Oxide and Other Catalysts for Ethane Conversion: A Review. *Catal. Today* **1999**, *51*, 379–348.
7. Talledo, A.; Granqvist, C. G. Electrochromic Vanadium Pentoxide Based Films: Structural, Electrochemical and Optical Properties. *J. Appl. Phys.* **1995**, *77*, 4655–4666.
8. Liu, P.; Lee, S. H.; Tracy, C. E.; Tuener, J. A.; Pitts, J. R.; Deb, S. K. Electrochromic and Chemochromic Performance of Mesoporous Thin-Film Vanadium Oxide. *Solid State Ionics* **2003**, *165*, 223–228.
9. Takahashi, K.; Wang, Y.; Cao, G. Z. Growth and Electrochromic Properties of Single-Crystal V_2O_5 Nanorod Arrays. *Appl. Phys. Lett.* **2005**, *86*, 053102.
10. Kudo, T.; Ikeda, Y.; Watanabe, T.; Hibino, M.; Miyayama, M.; Abe, H.; Kajita, K. Amorphous V_2O_5/Carbon Composites as Electrochemical Supercapacitor Electrodes. *Solid State Ionics* **2002**, *152*, 833–841.
11. Lee, H. Y.; Goodenough, J. B. Ideal Supercapacitor Behavior of Amorphous $V_2O_5 \cdot nH2_O$ in Potassium Chloride (KCl) Aqueous Solution. *J. Solid State Chem.* **1999**, *148*, 81–84.
12. Kim, I. H.; Kim, J. H.; Cho, B. W.; Lee, Y. H.; Kim, K. B. Synthesis and Electrochemical Characterization of Vanadium Oxide on Carbon Nanotube Film Substrate for Pseudocapacitor Applications. *J. Electrochem. Soc. A* **2006**, *153*, 989–996.
13. Coustier, F.; Hill, J.; Owens, B. B.; Passerini, S.; Smyrl, W. H. Doped Vanadium Oxides as Host Materials for Lithium Intercalation. *J. Electrochem. Soc.* **1999**, *146*, 1355–1360.
14. Crespi, A.; Schmidt, C.; Norton, J.; Chen, K.; Skarstad, P. Modeling and Characterization of the Resistance of Lithium/SVO Batteries for Implantable Cardioverter Defibrillators. *J. Electrochem. Soc.* **2001**, *148*, A30–A37.
15. Leising, R. A.; Takeuchi, E. S. Solid-State Synthesis and Characterization of Silver Vanadium Oxide for Use as a Cathode Material for Lithium Batteries. *Chem. Mater.* **1994**, *6*, 489–495.
16. Chu, Y. Q.; Qin, Q. Z. Fabrication and Characterization of Silver−V_2O_5 Composite Thin Films as Lithium-Ion Insertion Materials. *Chem. Mater.* **2002**, *14*, 3152–3157.
17. Zhang, J.; McGraw, J. M.; Turner, J.; Ginley, P. Charging Capacity and Cycling Stability of VO_x Films Prepared by Pulsed Laser Deposition. *J. Electrochem. Soc.* **1997**, *144*, 1630–1634.
18. Lee, J. M.; Hwang, H. S.; Cho, W-Il; Cho, B. W.; Kim, K. Y. Effect of Silver Co-Sputtering on Amorphous V_2O_5 Thin Films for Microbatteries. *J. Power Sources* **2004**, *136*, 122–131.
19. Gulbinski, W.; Suszko, T.; Sienicki, W.; Warcholinski, B. Tribological Properties of Silver and Copper Doped Transition Metal Oxide Coatings. *Wear* **2003**, *254*, 129–135.
20. Khan, G. A.; Hogarth, C. A. A. Conduction through MIM Sandwich Samples of Evaporated Thin Films of V_2O_5 and V_2O_5/B_2O_3. *J. Mater. Sci.* **1991**, *26*, 1087–1092.
21. Julien, C.; Guesdon, J. P.; Gorenstein, A.; Khelfa, A.; Ivanov, I. The Influence of the Substrate Material on the Growth of V_2O_5 Flash-Evaporated Films. *Appl. Surf. Sci.* **1995**, *90*, 389–391.
22. Wenda, E. Phase Diagram of V_2O_5-MoO_3-Ag_2O—I. Phase Diagram of V_2O_5-Ag2O System. *J. Therm. Anal.* **1985**, *30*, 879–887.
23. Takeuchi, K. J.; Leising, R. A.; Palazzo, M. J.; Marschilok, A. C.; Takeuchi, E. S. Advanced Lithium Batteries for Implantable Medical Devices: Mechanistic Study of SVO Cathode Synthesis. *J. Power Sources* **2003**, *119*, 73–978.
24. Zhang, S.; Li, W.; Li, C.; Chen, J. Synthesis, Characterization, and Electrochemical Properties of $Ag_2V_4O_{11}$ and $AgVO_3$ 1-D Nano/Microstructures. *J. Phys. Chem. B* **2006**, *110*, 24855–24863.
25. Shen, G.; Chen, D. Self-Coiling of $Ag_2V_4O_{11}$ Nanobelts into Perfect Nanorings and Microloops. *J. Am. Chem. Soc.* **2006**, *128*, 11762–11763.
26. Livage, J. Vanadium Pentoxide Gels. *Chem. Mater.* **1991**, *3*, 578–593.
27. Muster, J.; Kim, G. T.; Krstic, V. Electrical Transport through Individual Vanadium Pentoxide Nanowires. *Adv. Mater.* **2000**, *12*, 420–424.
28. Kim, G. T.; Muster, J.; Park, J. G.; Krstic, V.; Park, Y. W. Field-Effect Transistor Made of Individual V_2O_5 Nanofibers. *Appl. Phys. Lett.* **2000**, *76*, 1875–1877.
29. Lamarque-Forget, S.; Pelletier, O.; Dozov, I.; Davidson, P.; Martinot-Lagarde, P.; Livage, J. Electrooptic Effects in the Nematic and Isotropic Phases of Aqueous V_2O_5 Suspensions. *Adv. Mater.* **2000**, *12*, 1267–1270.
30. Kim, Y. K.; Park, S. J.; Koo, J. P.; Kim, G. T.; Hong, S.; Ha, J. S. Control of Adsorption and Alignment of V_2O_5 Nanowires via Chemically Functionalized Patterns. *Nanotechnology* **2007**, *18*, 015304.
31. Ancona, M. G.; Kooi, S. E.; Kruppa, W. A.; Snow, W.; Foos, E. E.; Whitman, L. J.; Park, D.; Shirey, L. Patterning of Narrow Au Nanocluster Lines using V_2O_5 Nanowire Masks and Ion-Beam Milling. *Nano Lett.* **2003**, *3*, 135–138.
32. Gu, G.; Schmid, M.; Chiu, P. W.; Minett, A.; Fraysse, J.; Kim, G. T.; Roth, S.; Kozlov, M.; Munõz, E.; Baughman, R. H. V_2O_5 Nanofibre Sheet Actuators. *Nat. Mater.* **2003**, *2*, 316–319.
33. Patzke, G. R.; Krumeich, F.; Nesper, R. Oxidic Nanotubes and Nanorods—Anisotropic Modules for a Future Nanotechnology. *Angew. Chem., Int. Ed.* **2002**, *41*, 2446–2461.

34. Niederberger, M.; Bard, M. H.; Stucky, G. D. Benzyl Alcohol and Transition Metal Chlorides as a Versatile Reaction System for the Nonaqueous and Low-Temperature Synthesis of Crystalline Nano-Objects with Controlled Dimensionality. *J. Am. Chem. Soc.* **2002**, *124*, 13642–13643.
35. Pinna, N.; Willinger, M.; Weiss, K.; Urban, J.; Schlögl, R. Local Structure of Nanoscopic Materials: V_2O_5 Nanorods and Nanowires. *Nano Lett.* **2003**, *3*, 1131–1134.
36. Cao, A. M.; Hu, J. S.; Liang, H. P.; Wan, L. J. Self-Assembled Vanadium Pentoxide (V_2O_5) Hollow Microspheres from Nanorods and their Application in Lithium-Ion Batteries. *Angew. Chem., Int. Ed.* **2005**, *44*, 4391–4395.
37. Livage, J. Synthesis of Polyoxovanadates via "Chimie Douce". *Coord. Chem. Rev.* **1998**, *178*, 999–1018.
38. Cazzanelli, E.; Mariotto, G.; Passerini, S.; Smyrl, W. H.; Gorenstein, A. Raman and XPS Characterization of Vanadium Oxide Thin Films Deposited by Reactive RF Sputtering. *Sol. Energy Mater. Sol. Cells* **1999**, *56*, 249–258.
39. Krishna, M. G.; Debauge, Y.; Bhattacharya, A. K. X-ray Photoelectron Spectroscopy and Spectral Transmittance Study of Stoichiometry in Sputtered Vanadium Oxide Films. *Thin Solid Films* **1998**, *312*, 116–122.
40. Rajendra Kumar, R. T.; Karunagaran, B.; Venkatachalam, S.; Mangalaraj, D.; Narayandass, S. K.; Kesavamoorthy, R. Influence of Deposition Temperature on the Growth of Vacuum Evaporated V_2O_5 Thin Films. *Mater. Lett.* **2003**, *57*, 3820–3825.
41. Ozer, N. Electrochemical Properties of Sol-Gel Deposited Vanadium Pentoxide Films. *Thin Solid Films* **1997**, *305*, 80–87.
42. Takahashi, K.; Wang, Y.; Lee, K.; Cao, G. Fabrication and Li^+-Intercalation Properties of V_2O_5-TiO_2 Composite Nanorod Arrays. *Appl. Phys. A: Mater. Sci. Process.* **2006**, *82*, 27–31.
43. Ivanova, T.; Harizanova, A. Electrochromic Investigation of Sol-Gel-Derived Thin Films of TiO_2-V_2O_5. *Mater. Res. Bull.* **2005**, *40*, 411–419.
44. Chen, W.; Kaneko, Y.; Kinomura, N. Preparation and Electrochromic Properties of V-Nb Mixed-Oxide Films by Evaporation. *J. Appl. Eletrochem.* **2003**, *32*, 515–518.
45. Huguenin, F.; Ferreira, M.; Zucolotto, V.; Franscisco, C. N.; Roberto, M. T.; Osvaldo, N. O., Jr. Molecular-Level Manipulation of V_2O_5/Polyaniline Layer-by-Layer Films to Control Electrochromogenic and Electrochemical Properties. *Chem. Mater.* **2004**, *16*, 2293–2299.
46. Cheng, K. C.; Chen, F. R.; Kai, J. J. V_2O_5 Nanowires as a Functional Material for Electrochromic Device. *Sol. Energy Mater. Sol. Cells* **2006**, *90*, 1156–1165.
47. Li, G. C.; Pang, S. P.; Jiang, L.; Guo, Z. Y.; Zhang, Z. K. Environmentally Friendly Chemical Route to Vanadium Oxide Single-Crystalline Nanobelts as a Cathode Material for Lithium-Ion Batteries. *J. Phys. Chem. B* **2006**, *110*, 9383–9386.
48. Liu, J.; Wang, X.; Peng, Q.; Li, Y. Vanadium Pentoxide Nanobelts: Highly Selective and Stable Ethanol Sensor Materials. *Adv. Mater.* **2005**, *17*, 764–767.
49. Liu, X.; Huang, C.; Qiu, J.; Wang, Y. The Effect of Thermal Annealing and Laser Irradiation on the Microstructure of Vanadium Oxide Nanotubes. *Appl. Surf. Sci.* **2006**, *253*, 2747–2751.
50. Huang, F.; Fu, Z. W.; Chu, Y. Q.; Liu, W. Y.; Qin, Q. Z. Characterization of Composite 0.5Ag:V_2O_5 Thin-Film Electrodes for Lithium-Ion Rocking Chair and All-Solid-State Batteries. *Electrochem. Solid State Lett.* **2004**, *7*, A180–A184.
51. Sanchez, C.; Livage, J.; Lucazeau, G. Infrared and Raman Study of Amorphous V_2O_5. *J. Raman Spectrosc.* **1982**, *12*, 68–72.
52. Vanova, T.; Harizanova, A. Electrochromic Investigation of Sol-Gel-Derived Thin Films of TiO_2-V_2O_5. *Mater. Res. Bull.* **2005**, *40*, 411–419.
53. Niederberger, M.; Muhr, H. J.; Krumeich, F.; Bieri, F.; Günther, D.; Nesper, R. Low-Cost Synthesis of Vanadium Oxide Nanotubes via Two Novel Non-alkoxide Routes. *Chem. Mater.* **2000**, *12*, 1995–2000.
54. Nordlinder, S.; Nyholm, L.; Gustafsson, T.; Edström, K. Lithium Insertion into Vanadium Oxide Nanotubes: Electrochemical and Structural Aspects. *Chem. Mater.* **2006**, *18*, 495–503.
55. Chaki, N. K.; Tsunoyama, H.; Negishi, Y.; Sakurai, H.; Tsukuda, T. Effect of Ag-Doping on the Catalytic Activity of Polymer-Stabilized Au Clusters in Aerobic Oxidation of Alcohol. *J. Phys. Chem. C* **2007**, *111*, 4885–4888.
56. Konova, P.; Arve, K.; Klingstedt, F.; Nikolov, P.; Naydenov, A.; Kumar, N.; Murzin, D. Yu. A Combination of Ag/Alumina and Ag Modified ZSM-5 to Remove NO_x and CO During Lean Conditions. *Appl. Catal. B: Environ.* **2007**, *70*, 138–145.
57. Cogan, S. F.; Nguyen, N. M.; Perrotti, S. J.; Rauh, D. R. Optical Properties of Electrochromic Vanadium Pentoxide. *J. Appl. Phys.* **1989**, *66*, 1333–1337.
58. Benmoussa, M.; Outzourhit, A.; Bennouna, A.; Ameziane, E. L. Electrochromism in Sputtered V_2O_5 Thin Films: Structural and Optical Studies. *Thin Solid Films* **2002**, *405*, 11–16.
59. Young, H. R.; Kiyoshi, K. Li^+-Ion Diffusion in $LiCoO_2$ Thin Film Prepared by the Poly(vinylpyrrolidone) Sol-Gel Method. *J. Electrochem. Soc.* **2004**, *151*, A1406–A1411.
60. Lantelme, F.; Mantoux, A.; Groult, H.; Lincot, D. Electrochemical Study of Phase Transition Processes in Lithium Insertion in V_2O_5 Electrodes. *J. Electrochem. Soc.* **2003**, *150*, A1202–1208.
61. McGraw, J.; Bahn, C.; Parilla, P.; Perkins, J.; Readey, D.; Ginley, D. Li ion Diffusion Measurements in V_2O_5 and $Li(Co_{1-x}Al_x)O_2$ Thin-Film Battery Cathodes. *Electrochim. Acta* **1999**, *45*, 187–196.
62. Julien, C.; Gorenstein, A.; Khelfa, A.; Guesdon, J. P.; Ivanov, I. Fabrication of V_2O_5 Thin Films and their Electrochemical Properties in Lithium Microbatteries. *Mater. Res. Soc. Symp. Proc.* **1995**, *369*, 639–647.
63. Seman, M.; Marino, J.; Yang, W.; Wolden, C. A. An Investigation of the Role of Plasma Conditions on the Deposition Rate of Electrochromic Vanadium Oxide Thin Films. *J. Non-Cryst. Solids* **2005**, *351*, 1987–1994.